Ro.Man.Sy 9
Udine, Italy 1992

A New Actuation System for High-Performance Torque-Controlled Manipulators

Robert Holmberg, Sanford Dickert, and Oussama Khatib
Robotics Laboratory
Department of Computer Science, Stanford University
Stanford, CA 94305, USA

Abstract

The work reported in this paper is a part of a larger effort concerned with the design and development of a high-performance force controlled, ten degree-of-freedom manipulator and mini-manipulator system, ARTISAN, currently under construction at Stanford University (Khatib, Roth and Waldron 1991). The paper focuses on the new actuation system developed for this robot. It discusses the design of the actuator-transmission-sensor system, describes the joint torque feedback controller, and presents experimental results obtained with a prototype of the wrist mechanism of ARTISAN.

Introduction

Proper implementation of dynamic motion control strategies involving gravity compensation, inertial decoupling, and centrifugal and coriolis compensation, as well as active force control strategies require the ability to precisely control individual joint torques. This ability, however, is considerably restricted by the nonlinearities and friction inherent in the actuator-transmission systems generally found in industrial robots.

There have been several efforts to improve joint torque control with joint torque sensing. Based on experiments with a single joint (Wu and Paul, 1980), the first two joints of a Stanford Arm were redesigned (Luh, Fisher, and Paul, 1983) to accommodate torque sensors. Joint torque sensory feedback has also been implemented in a direct-drive manipulator (Asada, Youcef-Toumi, and Lim, 1984) and in a PUMA manipulator (Pfeffer, Khatib, and Hake, 1986). These experiments have shown that, although joint friction effects can be substantially reduced by torque servoing, a wide joint actuation bandwidth is difficult to achieve without actually reducing the friction and non-linearities in the actuator-transmission system.

Another line of research has been directed at the development of *direct-drive* arms which eliminate transmission non-linearities. Since the first development of a direct-drive arm at CMU (Asada and Kanade 1983), several other designs have been proposed and direct-drive manipulators have become commercially available. However, direct-drive arms require relatively massive actuators. Additionally, direct-drive manipulators are more sensitive to dynamic coupling, and thus will be more susceptible to dynamic modeling errors and dynamic perturbations.

Our recent research has been guided by a list of desirable properties for high performance joint torque control which includes: high backdriveability, low friction, minimal effects of disturbance

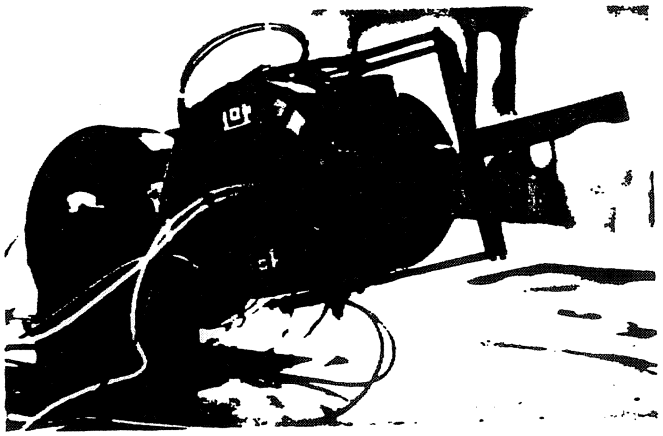

Figure 1: ARTISAN Wrist Mechanism

torques, and low backlash. To achieve these properties, a design with a low-ratio gear transmission system and joint torque feedback is currently being used in the development of ARTISAN (Vischer and Khatib 1989, 1990). The discussion in this paper will focus on developments related to the new prototype wrist mechanism of ARTISAN, as shown in Figure 1.

Actuator-Transmission Design

In the ARTISAN project there are two major design goals which affect the actuation system: The torque generated at each joint must be precisely controllable; and the actuation system must be small, light, and powerful enough to work within the given configuration. Direct-drive actuators have good torque control potential but are too large and heavy. The use of a single-stage gear transmission at each joint allows the size and weight of the motors to be minimized to fit into the ARTISAN design. Both the motors and the gears are selected so as to minimize their non-linearities.

The design tradeoffs between ratio, diameter, and load capacity faced when using single stage gear reduction are addressed through the use of *evoloid* gear sets for each joint (Berlinger 1975). Evoloid gears are very similar to helical spur gears except that coarser pitches are normally used. As with helical gears, evoloid gear sets are easily backdriveable and have smooth torque transfer characteristics. Evoloid pinions, however, are noticeably different from similarly sized helical spur gear pinions. Evoloid pinions have only a few (usually one to four) thick teeth. Because of the relatively thicker teeth on the pinion, evoloid gear sets have higher load capacities and better resistance to shock loads than helical gears. Figure 2 shows two pinions with similar tooth thicknesses, which

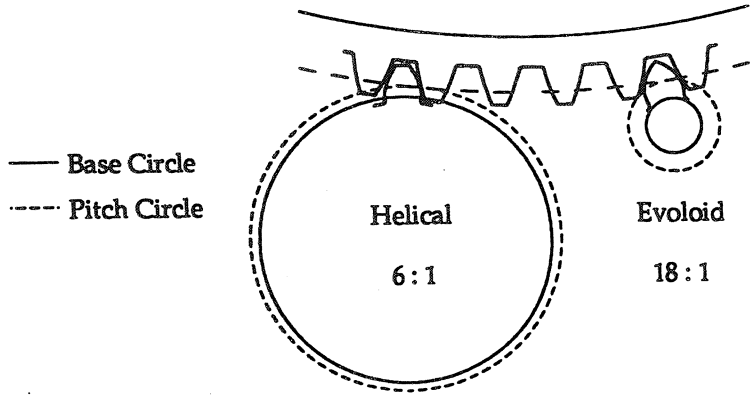

Figure 2: Comparison of Helical and Evoloid Pinion Profiles with Similar Load Capacities

translate into approximately similar load capacities. The three-fold increase in ratio of the evoloid set allows two possibilities: a significant increase in the gear output torque while keeping the gear size constant, or a significant decrease of the gear size while maintaining the same output torque capability as the helical set. We have taken advantage of the second possibility in our design. To illustrate, the previous ARTISAN prototype (Vischer and Khatib 1990) used 15.2 cm diameter, 6:1 helical gears. The evoloid gears used in the current prototype have smaller diameters of 12.2 cm and 14.1 cm, with higher ratios of 13.25:1 and 15:1. This is important since the size of the gears in the wrist is the limiting factor for reducing the girth of the arm.

At each joint, our current prototype uses a double-ended shaft in parallel with two single-stage evoloid gears to increase the torque that can be delivered to the joint. Each pair of pinions is driven directly by a high-power brushless DC motor using rare earth samarium-cobalt magnets. This arrangement gives a maximum payload of 8 Kg with a minimum of 4 g's available acceleration.

To reduce the effect of torque ripple generated by the motor, we use brushless DC motors with additional enhancements provided by the Inland Motor Company. Using brushless DC motors eliminates breakaway friction torques and electrical noise generated by sparking brushes. We have chosen motors with skewed stator windings to reduce the cogging torque generated by residual magnetic effects in the motor. The most significant reduction of torque variation is achieved by using sinusoidal commutation derived from a shaft-mounted encoder. The use of sinusoidal commutation, versus conventional six-step methods, reduces torque ripple by assuring continuous, smooth commutation to all windings, while compensating for the motor's sinusoidally varying torque constant. This technique reduces the torque ripple from 5-15% down to 3% or less (McCormick 1990).

Torque Sensor Design

Previous investigation of torque sensing devices resulted in a conceptually new torque sensor (Vischer and Khatib 1989) which obtains torques from measurements of beam deflections through the use of contact-free distance sensors.

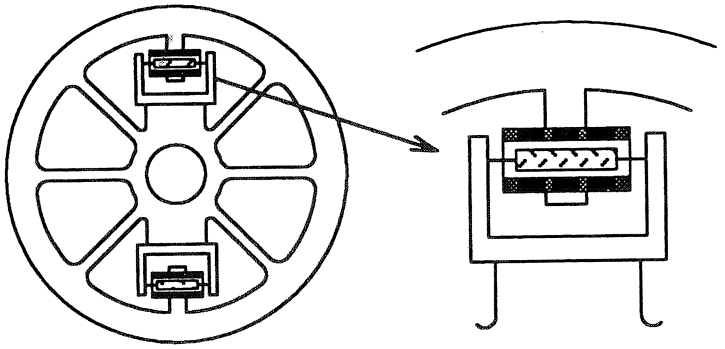

Figure 3: Six Beam Torque Sensor

The torque sensor illustrated in Figure 3 converts a torque applied to the central hub into a measurable displacement at each transducer location. The beams are arranged to give a lowered stiffness about the joint axis, while retaining much higher stiffnesses in other directions. The torque sensed, T_s, is linear with respect to the the angular deflection, θ_s, and is given by:

$$T_s = k\theta_s \tag{1}$$

where k, the sensor stiffness, is determined by the geometry and material of the sensor,

$$k = 4NEI\left(\frac{1}{l} + \frac{3r}{l^2} + \frac{3r^2}{l^3}\right) \tag{2}$$

with N = number of spokes, E = Young's modulus, I = spoke section modulus, l = spoke length, and r = sensor inner radius. The deflection of the spokes is used to calculate T_s by measuring the approximately linear displacement, Δx, created at the radius of the transducer, r_t, according to:

$$T_s = kr_t(\Delta x) \tag{3}$$

There are several constraints which affect the design of the spoke geometry and the transducer selection.

- The deflection at the maximum expected torque should not exceed the range of the transducer.
- The stiffness in directions other than the joint axis should be as high as possible.
- The flexibility of the spokes should not introduce a resonant frequency lower than frequencies of interest.

In the ARTISAN wrist prototype, the torque sensor has been removed from the gear and placed as either the first or last element of the joint transmission. This assures that the total torque between the joints is measured. As discussed in the earlier analysis of sensor placement (Vischer and Khatib 1990), this placement greatly reduces the disturbance effects of radial forces generated by the meshing of the gears. This location of the sensor, however, allows other forces from the link to cause sensor deflections. Due to sensor stiffness in the other directions, these deflections do not affect the torque measurements. Additionally, these defections are either perpendicular to the transducers and not measured, or they are cancelled out by subtracting the displacement measurements through a bridge configuration of the transducers.

Transducer Selection

With the above torque sensor design, a torque applied to the flexible spoked structure causes a predictable amount of deflection to occur. This deflection must then be transformed into an electrical signal This means that the selection of an appropriate transducer is paramount. Strain gauges, which are usually used in a force measurement application, were determined to be problematic in this application due to saturation (or breakage), installation, and electrical noise sensitivity.

The use of inductive transducers, as discussed in Vischer and Khatib 1990, provided greater robustness than the more frequently used strain gauge sensors due to their noise insensitivity and measurement range. In our further investigations, we found that we were able to measure finer displacements, with more repeatability, through the use of a linear variable differential transformer, or LVDT, from Lucas Schaevitz. Compared to the inductive transducers, the LVDTs we have selected provide a larger range of measurement and a similar theoretical resolution of about 0.1 μm. The LVDTs also allow for easier installation and calibration, greater mechanical stability. Our current sensor design is based on implementing these devices in the same manner as the previous inductive transducers (see Figure 3).

Both the inductive transducers and LVDTs use a modulated carrier signal which must be decoded. The open loop signal conditioners used with the inductive transducers produce an analog voltage which was subject to electrical noise and drift. To remedy this problem, we are using the Analog Devices 2S54 LVDT to Digital Converter. This product provides demodulation of the Wheatstone bridge signal and converts the quantity to a 14 bit word through the use of a Type II tracking loop and up/down counter. The tracking loop provides zero steady state error for the measurement of displacement and velocity which, in turn, corresponds to torque and its first derivative. The

tracking loop and digital format also provides immunity from the drift and noise problems that plague analog decoding electronics.

The use of the AD2S54 was not without cost, though — the system's Type II tracking loop results in a third order filter between the sensor and the computer. Since the tracking loop operates within the expected dynamic range, the design of a controller needs to include the effect of the transfer function in our analysis:

$$\frac{\Delta x_{signal}}{\Delta x_{deflect}} = \frac{T_1 s + 1}{\frac{T_2}{K_a} s^3 + \frac{1}{K_a} s^2 + T_1 s + 1} \tag{4}$$

where T_1, T_2, and K_a are determined by the particular model of converter.

Link Descriptions

The current ARTISAN prototype includes joints 5 and 6 (out of 10) and these together may be considered the arm's wrist. They are the two base links of the six-degree-of-freedom mini manipulator now under construction. These two axes are perpendicular and intersecting. Joint 5 has a 65° range of motion and joint 6 can move a full 180°. They are supported by the link 4 structure which is fixtured to the ground (see Figure 1).

The dynamics of each link involve forces from the motor, link inertia, motor inertia, and internal frictions. The equations of motion for each link have been generated independently as the foundation for a set of independent joint torque controllers. Using the symbols in Table 1, the equations for joint 5 are:

$$J_m \ddot{\theta}_m = T_m + \left(\dot{\theta}_l - \dot{\theta}_m\right) d_m + \frac{T_s}{N} \tag{5}$$

$$J_e \ddot{\theta}_l = -T_m + \left(\dot{\theta}_s - \dot{\theta}_l\right) d_l + \left(\dot{\theta}_m - \dot{\theta}_l\right) d_m - T_s \left(1 + \frac{1}{N}\right) \tag{6}$$

$$\theta_m = -\left(\theta_s N\right) + \theta_l \left(1 + N\right) \tag{7}$$

where J_e is the equivalent inertia of the link and motor.

$$J_e = J_l + mC^2 \tag{8}$$

The equations for joint 6:

$$T_m = J_m \ddot{\theta}_m + \dot{\theta}_m d_m - \frac{T_s}{N} - \left(\dot{\theta}_l + \dot{\theta}_s\right) \frac{d_l}{N} \tag{9}$$

$$J_l \ddot{\theta}_l = T_s \tag{10}$$

$$\theta_m = -\left(\theta_l N\right) - \theta_s N \tag{11}$$

N	Gear Ratio	J_m	Motor Inertia	θ_s	Sensor Deflection
k	Sensor Stiffness	J_l	Link Inertia	θ_l	Link Angle
C	Center Distance	J_e	Equiv. Inertia	θ_m	Motor Angle
m	Motor Mass	T_s	Sensor Torque	d_l	Link Friction
		T_m	Motor Torque	d_m	Motor Friction

Table 1: Link Parameters

Torque Transfer Function

The torque transfer function for each joint can be obtained from the joint equations of motion. The equation for joint 5 from (1), (5), (6), and (7) is:

$$\frac{T_s}{T_m} = -\frac{\left(\frac{k}{J_e} + \frac{k}{J_m N} + \frac{k}{J_e N}\right) s + \frac{d_l k}{J_m J_e N}}{s^3 + \left(\frac{d_m}{J_m} + \frac{d_m}{J_e} - \frac{d_l}{J_e N}\right) s^2 + \left(\frac{k}{J_e} + \frac{k}{J_m N^2} + \frac{k}{J_e N^2} + \frac{2k}{J_e N}\right) s + \left(\frac{d_m k}{J_m J_e} + \frac{d_l k}{J_m J_e N^2}\right)} \tag{12}$$

Experimental frequency responses have shown the system to have dominant second order character with weak damping. To simplify analysis, an approximation can be made then by assuming $d_l = d_m = 0$ in (12) and simplifying the transfer function to:

$$\frac{T_s}{T_m} = -\frac{\frac{k}{J_e} + \frac{k}{J_m N} + \frac{k}{J_e N}}{s^2 + \left(\frac{k}{J_e} + \frac{k}{J_m N^2} + \frac{k}{J_e N^2} + \frac{2k}{J_e N}\right)} \tag{13}$$

The torque transfer function for joint 6 is obtained in the same manner, from (1), (9), (10), and (11):

$$\frac{T_s}{T_m} = -\frac{\frac{k}{J_m N} s}{s^3 + \left(\frac{d_m}{J_m} + \frac{d_l}{J_m N^2}\right) s^2 + \left(\frac{k}{J_l} + \frac{k}{J_m N^2}\right) s + \left(\frac{d_m k}{J_l J_m} + \frac{d_l k}{J_l J_m N^2}\right)} \tag{14}$$

and by assuming $d_l = d_m = 0$, (14) reduces to:

$$\frac{T_s}{T_m} = -\frac{\frac{k}{J_m N}}{s^2 + \left(\frac{k}{J_l} + \frac{k}{J_m N^2}\right)} \tag{15}$$

Controller Design

The intent of our control design is to close a fast torque servo loop around each joint, and then close a position loop about each joint. Once the torque loop is in effect, the joint motor and transmission should seem like a pure torque source, providing enhanced performance in responding to torque commands from the position servo.

Since our design goal was to construct as simple a torque loop as possible, we approximated the two joints to have the simple second order transfer functions expressed in (13) and (15). By ignoring the effects of the sensor electronics, a simple lead compensator could provide the desired bandwidth for the torque servo loop.

During experimentation and frequency analysis, the effect of the sensor electronics and structural resonances of the wrist were found to limit the performance of the torque loop. Therefore, we returned to the practice of prefiltering the input and filtering the feedback to frequencies below the lowest structural resonance, in order to closely approximate a simple gain. The selection of the cutoff frequencies of the filters were a tradeoff between servo bandwidth and controller complexity.

Using this filtering technique, the open loop transfer function could then be approximated by:

$$T_s = k_0(NT_m + T_d). \tag{16}$$

where T_d are the disturbances that act upon the sensor from the motor and the link. But due to the sensor electronics and structural resonances, the above approximation did not conform to the experimental prototype. Therefore, a simple PID controller was designed and tested.

Experimental Data

By performing a frequency analysis on the two joints, we were able to compare the theoretical sensor modes to the actual ones. Through this analysis, we found that the second order approximations, (13) and (15), were useful in determining the natural frequency of each joint. Additionally, we were able to ascertain a structural resonance mode at 33 Hz, which provided an upper bound on the possible bandwidth of the torque loop.

By installing four LVDTs per joint in the prototype wrist and utilizing one AD2S54 per LVDT, the sensor sensitivity is shown in Table 2. All measurements have an ambient noise floor of one quanta.

Joint	Sensitivity at Joint
5	0.00251 N·m
6	0.00268 N·m

Table 2: Six Beam / LVDT Sensor Sensitivity

By using the following PID compensators, listed in Table 3, and utilizing the new sensor electronics and transducers, we have completed a zero-torque controller which is successful in greatly reducing friction and disturbances while enhancing backdrivability. In addition, we have closed a position loop around each torque servo to enhance the performance of each position loop. By using both joints 5 and 6, we have demonstrated improvement in tracking a circular trajectory as shown in the intermediary results of Figure 4.

Joint 5 Compensator	Joint 6 Compensator
$\frac{1.4521z^2-2.5538z+1.1857}{z^2-0.988z}$	$\frac{1.7451z^2-2.7101z+1.0375}{z^2-0.988z}$

Table 3: PID Compensators for Joints 5 and 6

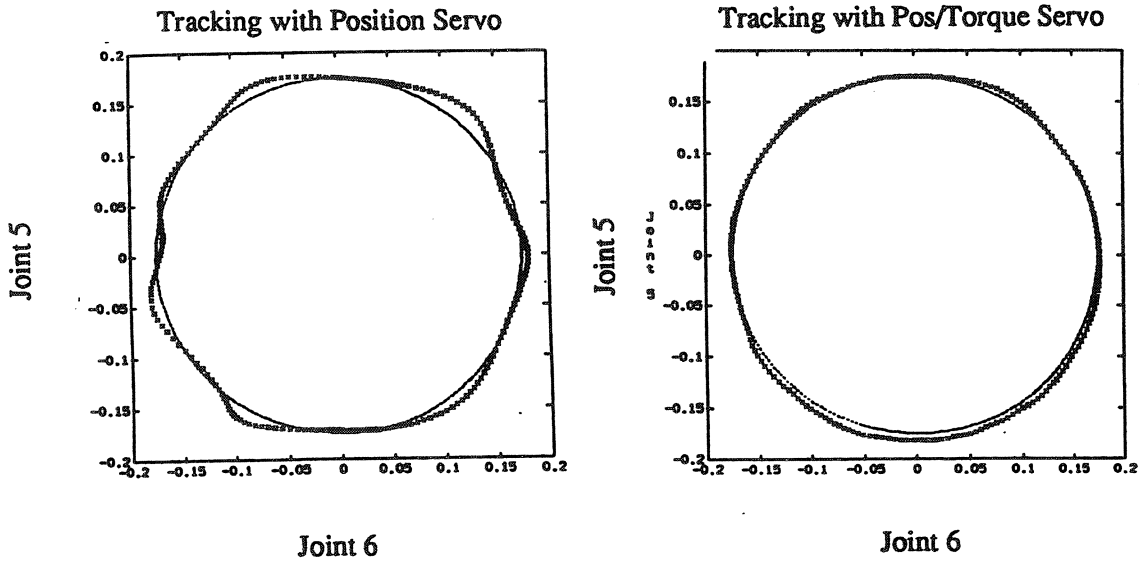

Figure 4: Circle Tracking Without/With Torque Servo; Dashed=Desired, X=Actual

Conclusions

The combination of single-stage evoloid gears and enhanced brushless DC motors produces a powerful, compact, and smooth torque actuation system. Spoked, integral, torque sensors allow us to reliably monitor the precise torque transferred to each link. These sensors are robust and have good disturbance rejection properties. The introduced flexibility creates a system with well behaved, second order, characteristics which can be closely modelled. The accuracy of our model was verified using frequency analysis. A simple PID controller with filtering was designed and implemented with good overall performance. Further exploration of advanced compensations and inverse filtering to minimize the effect of the sensor electronics is currently in progress.

Acknowledgements

The financial support of SIMA, GM, and Toyota are acknowledged. We are thankful to Professors Bernard Roth and Kenneth Waldron and to Bill Bencze, Bernard Berlinger, Bryan Dishner, Alain Fidani, Matthew Finnie, Malcolm McCormick, John Meadows, and Sean Quinlan who have made valuable contributions to the development of this work. *Evoloid* is a trademark used by ASI Technologies.

References

Asada, H., and Kanade, T. 1983, "Design of Direct-Drive Mechanical Arms," *ASME Journal of Vibration, Acoustics, Stress, and Reliability in Design,* 105(3), pp. 312-316.

Asada, H., Youcef-Toumi, K., and Lim, S.K., 1984, "Joint Torque Measurement of a Direct-Drive Arm," *Proceedings of the 23rd IEEE Conference on Decision and Control,* pp. 1332-1337, Las Vegas.

Berlinger, B.E. Jr., 1975, "EVOLOID — A New Concept in High Ratio Gearing," AGMA Paper No. 109.37, October 1975.

Khatib, O., Roth, O., and Waldron, K.J., 1991, "The Design of a High-Performance Force-Controlled Manipulator," *Proc. Eighth IFToMM World Congress on the Theory of Machines and Mechanisms,*, Prague, Czechoslovakia, vol. 2, pp. 475-478.

Luh, J.Y.S., Fisher, W.B., and Paul, R.P., 1983, "Joint Torque Control by Direct Feedback for Industrial Robots," The IEEE Transactions on Automatic Control, vol. AC-28, No 2.

McCormick, Malcolm, B., 1990, "Sinusoidal Commutation Cuts Torque Ripple in Brushless DC Motors," PCIM Magazine, June, 1990.

Pfeffer, L., Khatib, O., and Hake, J., 1986, "Joint Torque Sensory Feedback in the Control of a PUMA Manipulator," *Proc. American Control Conference,* Seattle, Washington, pp. 818-824.

Vischer, D., and Khatib, O., 1990, "Design and Development of Torque-Controlled Joints," *Experimental Robotics I,* Hayward, V. and Khatib, O. (Eds.), Springer-Verlag Berlin Heidelberg, pp. 271-286.

Wu, C.H. and Paul,R.P., 1980, "Manipulator Compliance Based on Joint Torque Control," *Proceedings of the 19th IEEE Conference on Decision and Control,* vol. 1, pp. 84-88, Albuquerque, New Mexico.